

ICNMM2008-62225

NUMERICAL INVESTIGATION ON FLOW PATTERN AND PRESSURE DROP CHARACTERISTICS OF SLUG FLOW IN A MICRO TUBE

Qunwu He

Department of Mechanical Engineering, The University of Tokyo, qwhe@thtlab.t.u-tokyo.ac.jp

Nobuhide Kasagi

Department of Mechanical Engineering, The University of Tokyo, kasagi@thtlab.t.u-tokyo.ac.jp

ABSTRACT

In the present study, numerical simulation of adiabatic air-water slug flow in a micro tube is carried out. The focus is laid upon the pressure drop characteristics and its modeling. The Phase-Field method is employed to capture the interface between the phases, while the surface tension force is represented by the chemical potential formulation. The numerical results agree fairly well with available experimental results in terms of bubble shape and flow pattern.

Simulation is repeated under different conditions of pressure gradient, void fraction and bubble frequency. It is found that the total pressure drop of a slug flow can be decomposed into two parts, i.e., the frictional pressure drop associated with a liquid slug sandwiched by bubbles, and the pressure drop over a bubble itself. For the former, when the liquid slug is longer than one tube diameter, the cross-sectional velocity distribution resembles a Poiseuille flow profile, so that the corresponding pressure drop can be predicted by the theoretical solution of single-phase liquid flow, i.e., $fRe_{TP} = 64$. For the latter, if it is assumed that the surface tension force is strong enough to sustain a thin liquid film between the interface and the tube wall, the pressure drop in this region is negligible. The pressure drop over a bubble is solely dependent on the two-phase superficial Reynolds number Re_{TP} , which can be correlated as: $\Delta p'_{bubb} = 0.07 + 42.4 / Re_{TP}$. This correlation predicts well the two-phase pressure drop in the form of the two-phase multiplier correlation as a function of the Lockhart-Martinelli parameter.

INTRODUCTION

Gas-liquid slug flow in micro conduits has attracted much attention because of its wide industrial applications such as micro heat exchangers and biotechnology systems. The features of extremely large surface-to-volume ratio, dominance of surface tension force, and alternate passage of gas and liquid provide a novel way for heat and mass transfer enhancement.

To optimize micro thermo-fluid systems, detailed understandings of flow and heat transfer mechanisms are crucial.

With order-of-magnitudes reduction in hydraulic diameter from 10 mm to 100 μm , significant differences in two-phase flow pattern, void fraction, pressure drop as well as heat/mass transfer have been reported. As reviewed by Ghiaasiaan S. M. (2001), although extensive experiments have been carried out, considerable discrepancies largely due to the difficulties in experimental setup and local measurements prevent to draw satisfied conclusions.

As an alternate way of investigation, numerical simulation provides possibilities to obtain local velocity and temperature in detail, and interpret the underlying physics. However, numerical simulation of two-phase flow in a micro conduit has been demonstrated to be a formidable task. The dominant surface tension force, abrupt changes of density over interface as well as the interaction between interface and solid wall set up great challenges for simulation. Continuous efforts have been made in the fields of interface tracking, surface tension formulation and transport model across interface. Son and Dhir (1999) developed a two-dimensional numerical model of growth and departure of single vapor bubble during nucleate pool boiling. They used the lubrication theory for phase change in microlayer region. Fukagata et al. (2007) simulated slug flows in a micro tube of 20 μm tube by using the level-set method to capture the interface, and higher pressure drop than that from experimental correlations was reported. By using CFD package CFX, Baten and Krishna (2005) investigated mass transfer from the liquid phase to the wall during the rise of Taylor bubbles in tubes of millimeter. A correlation was proposed for practical estimation of wall mass transfer.

Usually, a circular tube with diameter from about 10 to several hundred μm is defined as a micro tube. With the reduction of scale, the surface tension force rather than the

body force dominates the flow and heat transfer performances. The resulting capillary number (Ca) for a typical slug flow is on the order of 0.001 ~ 0.1. Due to the large interface curvature, the pressure jump across the interface between the liquid and gas phases is significant. When the surface tension force is discretized with finite grids, tiny numerical errors will cause a considerable parasitic flow when conventional continuum surface force (CSF) model is being used (Shirani et al. 2005), although it has been widely employed in various interface-capturing methods such as level-set and volume-of-fluid (VOF) method.

As an alternative approach, the so-called Phase-Field method describes the fluids and the interface from the viewpoint of energy. The surface tension force is correspondingly represented as the extra potential energy due to the variation of fluid density across the interface. With the exact conservation of surface tension energy and kinetic energy, the chemical potential formulation of the surface tension force in the frame of Phase-Field method can reduce the parasitic flow to the level of the truncation error (He et al. 2008).

Our final goal is to perform systematic simulations of two-phase flow in micro conduits in order to understand the two-phase flow and heat transfer mechanisms. In the present work, the Phase-Field method is employed to simulate gas-liquid two-phase slug flows without phase change in a micro tube; the flow characteristics are compared with available experimental results. The pressure drop mechanism is studied and a more reasonable model to take the bubble frequency into account is proposed and evaluated.

NOMENCLATURE

C	Chisholm parameter
Ca	capillary number
Cn	Cahn number
D	tube diameter (mm)
F	concentration
\vec{F}_s	surface force (N)
j	superficial velocity (ms^{-1})
L	length (m)
M	mobility
p	pressure (Nm^{-2})
Pe	Peclet number
r	radial coordinate (m)
R	tube radius (m)
Re	two-phase Reynolds number
t	time (s)
u	local velocity (ms^{-1})
U	average velocity (ms^{-1})
V	volume
We	Weber number
X	Martinelli parameter
z	longitudinal coordinate (m)

Greek letters

ρ	density (kgm^{-3})
μ	viscosity (Pas)
ϕ	chemical potential

Φ_L^2	two-phase multiplier
Ψ	free energy density (J)
Ω	domain
ψ	dimensionless stream function
ε	interface thickness parameter
σ	surface tension coefficient (Nm^{-1})
γ	constant $6\sqrt{2}$
α	void fraction
β	volumetric gas flow ratio

Subscripts

c	characteristic values
cap	bubble caps
eq	equilibrium
equ	equivalent
film	liquid film region
G	gas phase
GO	gas-only
L	liquid phase
LO	liquid-only
TP	two-phase
bubb	gas bubble
slug	liquid slug
fri	friction
wall	values at wall
f	front of bubble
r	rear of bubble
z	longitudinal

SIMULATION METHOD

Interface Capturing Method

Phase-Field method (Jacqmin 1999) is a kind of diffuse-interface method, which replaces a sharp fluid interface by a thin but nonzero thickness transition region. The interfacial forces are thereby smoothly distributed. The basic idea is to introduce a conserved order parameter, F , to characterize the two different phases, and it is analogous to the relative concentration between the two phases. The F assumes to have a distinct constant value in each bulk phase and changes rapidly but smoothly in the interfacial region. In the present study, the liquid takes the value of $F = 1$, while the gas $F = 0$. The transition from 1 to 0 represents the interface region. The concentration F is governed by the Cahn-Hilliard (C - H) equation, i.e.,

$$\frac{\partial F}{\partial t} + (\vec{u} \cdot \nabla)F = \nabla \cdot (M(F)\nabla\phi) , \quad (1)$$

$$\phi = \Psi'(F) - \varepsilon^2 \nabla^2 F , \quad (2)$$

where $M(F)$, $\Psi(F)$ and ε are the mobility, bulk energy density and interface thickness parameter, respectively. For simplicity, the mobility $M(F)$ is assumed to be a constant in the present study. The bulk energy density $\Psi(F)$ is defined as $F^2(1-F^2)/4$, which is a double-well positive function and has two minima corresponding to the two stable phases. The immiscibility of the fluid components has also been modeled thereby. The chemical potential, ϕ , is the rate of change of free energy with respect to F . Accordingly, the equilibrium interface profiles are the

solutions when ϕ is constant. It has been shown that the classical Navier-Stokes equations and pressure jump conditions are recovered in the sharp interface limit $\varepsilon \rightarrow 0$ (Anderson et al. 1998).

Governing Equations

Once the shape and position of an interface is calculated from Eq. (1), the physical properties of fluids are calculated by interpolating those of gas and liquid phases, i.e.,

$$\rho = \rho_L F + \rho_G (1 - F), \quad \mu = \mu_L F + \mu_G (1 - F), \quad (3)$$

where ρ and μ denote the density and viscosity, and the subscripts L and G represent the liquid and gas, respectively.

An isothermal air-water two-phase flow in a cylindrical pipe is considered. It is assumed that the gas and liquid are immiscible and phase change does not take place. Under these assumptions, the governing equations are written as follows:

$$\nabla \cdot \bar{u} = 0, \quad (4)$$

$$\frac{\partial(\rho \bar{u})}{\partial t} + \bar{u} \cdot \nabla(\rho \bar{u}) = -\nabla p + \nabla \cdot [\mu(\nabla \bar{u} + (\nabla \bar{u})^T)] + \bar{F}_s. \quad (5)$$

The gravity force is neglected because of a very small tube diameter considered. The surface tension force, \bar{F}_s , appearing in Eq. (5) is computed by using the chemical potential formulation (Jacqmin 1999):

$$\bar{F}_s = -\frac{\sigma \gamma}{\varepsilon} F \nabla \phi, \quad (6)$$

where σ denotes the surface tension coefficient. Equation (6) ensures that the change rate of free energy due to convection has the same magnitude, but an opposite sign to the change rate of kinetic energy due to surface tension (Jacqmin 1999). Assuming the concentration F to be locally equilibrium during evolution and also to match the surface tension of the sharp interface model, γ in Eq. (6) must satisfy

$$\varepsilon \gamma \int_{-\infty}^{\infty} (F_{eq}(x))^2 dx = 1. \quad (7)$$

The one-dimensional (say, along the x -direction) non-uniform solution gives the equilibrium composition profile as:

$$F_{eq}(x) = \frac{1 + \tanh(x / 2\sqrt{2}\varepsilon)}{2}, \quad (8)$$

and $\gamma = 6\sqrt{2}$ as was first obtained by van der Waals.

Nondimensionalization

We define the dimensionless variables as

$$r' = \frac{r}{L_c}, \quad z' = \frac{z}{L_c}, \quad u' = \frac{u}{U_c}, \quad t' = \frac{t U_c}{L_c}, \quad p' = \frac{p}{\rho_c U_c^2},$$

where L_c is the characteristic length, which is taken to be the radius of tube in the present study, U_c is the characteristic velocity, and ρ_c is the characteristic density defined as that of liquid. Dropping the primes, the dimensionless equations read

$$\begin{aligned} \nabla \cdot \bar{u} &= 0, \\ \frac{\partial(\rho \bar{u})}{\partial t} + \bar{u} \cdot (\nabla \rho \bar{u}) &= -\nabla p + \frac{1}{Re} \nabla \cdot (\mu(F)(\nabla \bar{u} + (\nabla \bar{u})^T)) - \frac{\sigma \gamma}{\varepsilon We} F \nabla \phi, \\ \frac{\partial F}{\partial t} + \bar{u} \cdot \nabla F &= \frac{1}{Pe} \nabla^2 \phi, \\ \phi &= \Psi'(F) - Cn^2 \nabla^2 F. \end{aligned} \quad (9)$$

The dimensionless parameters of Reynolds number Re , the

Peclet number Pe and the Weber number We are defined as

$$Re = \frac{\rho_c U_c L_c}{\mu_c}, \quad Pe_F = \frac{U_c L_c}{M_c \phi_c}, \quad We = \frac{\rho_c U_c^2 L_c}{\sigma}. \quad (10)$$

The Reynolds number is the ratio between inertial and viscous forces, the diffusional Peclet number is that between convective and diffusive mass transport, and the Weber number is the force ratio of inertia and surface tension. The Cahn number,

$$Cn = \varepsilon / L_c, \quad (11)$$

is a dimensionless numerical parameter that provides a measure of the ratio between the interface thickness and the characteristic length L_c . The choice of Cn is influenced by the numerical accuracy, efficiency and stability (Jacqmin 1999).

Numerical Procedures

The Navier-Stokes equations are solved by the SMAC method. A constant pressure gradient, $-dP/dz$, is applied in the z direction. The second-order central difference scheme is used for the spatial discretization. The pressure Poisson equation is solved by the successive over-relaxation (SOR) scheme. An equally spaced staggered grid system is adopted. The grid is uniform both in the longitudinal (z) and radial (r) directions. The grid size is fixed at $\Delta r/R = \Delta z/R = 0.03125$, which corresponds to 32 grids in the radial direction. Considering the steep change of F across the interface, advection term of Eq. (1) is solved by the CIP scheme, which is compact, bounded and of nearly spectral accuracy (Yabe et al. 1991). The right-hand-side terms of Eqs. (1) and (2) are discretized by using the standard central difference scheme.

Simulation Conditions

We consider a slug flow of air and water in a micro tube, and an axisymmetric flow is assumed. The flow consists of a periodic train of bubbles, which occupies most of the tube cross-section. It has been reported by many experimental visualizations that the gas bubbles and liquid slugs appear to stay a constant length and travel at the same velocity in a micro tube (Hayashi et al. 2007, Amador et al. 2004). Agglomeration and coalescence only take place at the entrance region. Therefore, the gas and liquid flow rate, and also the inlet geometry together determine the gas bubble and liquid slug lengths. The observation indicates that a model without agglomeration would be reasonable for slug flow in micro tubes.

The bubble frequency, i.e., the number of gas bubble and liquid slug pairs in unit tube length, is represented in terms of length of period L_z/R , where R is the tube radius, and it varies as $L_z/R = 3-15$ in the present simulations. The computational domain is two-dimensional ($r - z$) with periodic boundary condition in the streamwise direction, z , and no-slip condition at the wall. Besides that, various boundary conditions are needed for C-H equation. The first one is for the chemical potential ϕ . By applying the divergence theorem to Eq. (1) and integrating it over the domain, Ω , we have,

$$\int_{\Omega} \frac{\partial F}{\partial t} dV + \int_{\partial \Omega} (\bar{u} \cdot \bar{n}) F dS = \frac{1}{M} \int_{\partial \Omega} \nabla \phi \cdot \bar{n} dS. \quad (12)$$

Under the no-slip boundary condition (i.e., $\bar{u} \cdot \bar{n} = 0$) and the conservation of mass in Ω , ($\int_{\Omega} \partial F / \partial t dV = 0$), the chemical potential has to satisfy the no-flux boundary conditions,

$$\bar{n} \cdot \nabla \phi = 0. \quad (13)$$

The second boundary condition for the concentration F depends on macroscopic contact angle at the contact-line region of three phases. For diffusively controlled local equilibrium at the wall, a contact angle is specified as (Jacqmin 1999):

$$\varepsilon \sigma \gamma \frac{\partial F}{\partial x_n} + \gamma_w g'(F) = 0. \quad (14)$$

The experimental visualizations (Hayashi et al. 2007, Kawahara et al. 2002) show that there always exists a liquid film separating the gas bubble from the solid wall. Therefore, complete wetting condition is applied along the wall in all simulations; namely, at the first line of computational nodes adjacent to the wall, the fluid is assumed as liquid.

In accordance with the experimental conditions by Hayashi et al. (2007), the water and Nitrogen at 20 °C (293 K) and 1 atm ($\rho_L = 1.0 \times 10^3 \text{ kg/m}^3$, $\mu_L = 8.9 \times 10^{-4} \text{ Pa}\cdot\text{s}$; $\rho_G = 1.2 \text{ kg/m}^3$, $\mu_G = 1.8 \times 10^{-5} \text{ Pa}\cdot\text{s}$) are used as working fluids. The resulting surface tension is 0.0728 N/m. The diameter of the cylindrical tube D is fixed at 600 μm . It should be noted that, unlike the experiment, the present simulation is run with the void fraction, bubble frequency and average pressure gradient being specific. The flow rate and local pressure drop are obtained after the simulation is converged.

RESULTS AND DISCUSSIONS

Flow Pattern

Initially, a preliminary case with sufficiently long gas bubble and liquid slug is carried out with $L_z/R = 15$. The resultant two-phase Reynolds number Re_{TP} is 458, which is defined as $Re_{TP} = \rho_L U_{TP} D / \mu_L$, where the U_{TP} is the sum of superficial gas and liquid velocities, i.e., $U_{TP} = j_G + j_L$. Due to the incompressibility assumption, the average velocity at each cross-section of the tube is equal to U_{TP} . Figure 1 shows the calculated bubble shape and contours of dimensionless stream function relative the bubble velocity ψ , defined as:

$$\frac{1}{r} \frac{\partial \psi}{\partial r} = u_z - U_{bubb}, \quad \frac{1}{r} \frac{\partial \psi}{\partial z} = -u_r. \quad (15)$$

Here U_{bubb} is the calculated bubble moving velocity, which can be visualized and recorded by high-speed camera in experiment. Because of the strong surface tension force ($Ca = \mu_L U_{TP} / \sigma = 0.003$), the cap of gas bubble is nearly spherical and the interface is rather close to the solid wall. Dry-out or contact is not formed due to the wetting condition assumed along the wall. Because of the presence of gas bubble, the flow structure is quite different from that of single-phase flow. As shown in Fig. 1, an anti-clockwise circulation is found inside the gas phase, with a relatively small clockwise circulation accompanied in the front part of gas bubble. A circulation can also be found in

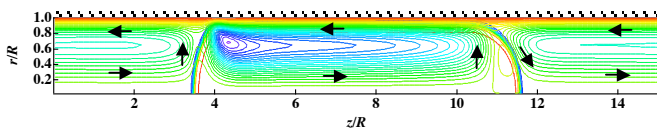


Fig. 1. Bubble shape and relative streamlines. The lines of $\psi < 0$ accords to clockwise circulation, as denoted by red lines, and $\psi > 0$ accords to anti-clockwise circulation denoted by blue.

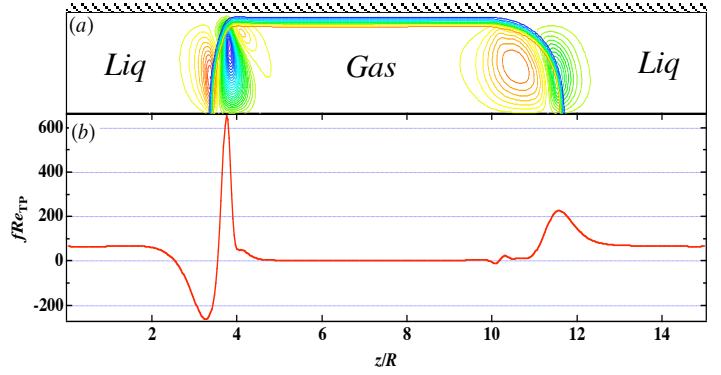


Fig. 2. Contours of normal velocity component (a) and axial variation of fRe_{TP} (b).

the liquid region, in accordance with the sketch of possible streamlines given by Taylor (1961). Similar results have been shown experimentally by Thulasidas et al. (1997) and numerically by Irandoust et al. (1989). This circulation results in continuous refreshment of the liquid layer near the wall and enhancement of heat and mass transfer.

It is well known that the circulations in both gas and liquid phases are due to the relative higher velocity at the tube center. When the fast flowing fluid at tube center encounters the interface, it bifurcates and flows perpendicularly towards the wall. This wall-normal velocity causes axial mixing as well as pressure deviation from that of single-phase flow. Figure 2 shows the contours of normal velocity components, u_r , and the variation of local fRe_{TP} number, where the friction factor is defined as:

$$f = \frac{(dp/dz)|_{wall} D}{\rho_L U_{TP}^2 / 2}. \quad (16)$$

As expected, u_r is detectable only in the region close to the bubble caps, and asymptotic to zero in the gas and liquid region. With the disappearance of u_r , the local value fRe_{TP} in the region of gas bubble is almost zero because of the stationary film between the interface and the solid wall. In the liquid slug region, $fRe_{TP} \approx 64$, and this indicates that the flow in this region resembles a Poiseuille flow and the velocity profile is independent of the location as:

$$\frac{u_z(r)}{U_{TP}} = 2(1 - (r/R)^2). \quad (17)$$

The features shown above suggest that it is possible to model the pressure drop of two-phase slug flow by decomposition, that is, the pressure drop over different regions can be modeled separately as a single phase liquid flow region and a bubble/liquid film region. The magnitude of normal velocity component can be employed as an indicator for the separating position. The details are discussed later.

The above simulation is repeated under different values of void fraction, α , pressure gradient, $-dP/dz$ and bubble frequency (length of period, L_z/R). Figure 3 shows the resultant relationship between the void fraction, α , and the gas volumetric flow ratio, β , which is defined as:

$$\beta = \frac{j_G}{j_G + j_L} = \alpha \frac{U_{bubb}}{U_{TP}}. \quad (18)$$

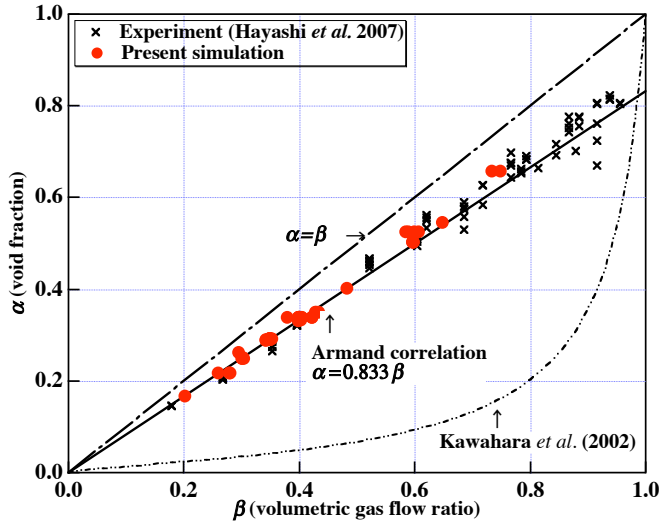


Fig. 3. Relationship between volumetric gas flow ratio (β) and void fraction (α)

As shown in the figure, the simulated cases lie along the so-called Armand correlation, which is proposed for conventional macro-sized tube,

$$\alpha = 0.833\beta. \quad (19)$$

By combining Eqs. (18) and (19), it straightforwardly leads to the relation of U_{bubb} to U_{TP} as follows:

$$\frac{U_{bubb}}{U_{TP}} \approx 1.2, \quad (20)$$

which implies that the bubble velocity is about 1.2 times that of the two-phase average velocity. The higher gas velocity corresponds to the centerline velocity in the tube. Hayashi et al. (2007) visualized the two-phase flow patterns, focusing on the bubbly and slug flow regimes. The slip ratio between U_{bubb} and U_{TP} is obtained by measuring the gas bubble velocity with a high-speed camera and U_{TP} at the inlet. The results are also shown in the figure, where the results of simulation and experiment agree fairly well. Kawahara et al. (2002) also proposed a correlation based on the experimental data for a 100 μm ID tube as:

$$\alpha = \frac{0.03\beta^{0.5}}{1 - 0.97\beta^{0.5}}. \quad (21)$$

In this correlation, α is a strongly nonlinear function of β because of the different flow patterns. Their reported two-flow patterns include quasi-annular and slug flows with long gas bubble. These flow patterns are the main reason for relatively high slip velocity between the phases.

Unit Cell Model

A large number of experimental results on two-phase pressure drop have been reported by employing the form of homogenous model or separated model like Lockhart-Martinelli (L-M) method. These models would be convenient in engineering practice. However, neither of them includes the information about the two-phase flow pattern. The significant pressure drop caused by bubbles would profoundly affect the overall pressure drop, as has been confirmed by several experimental (Fukano et al. 1993, Saisorn et al. 2007) as well

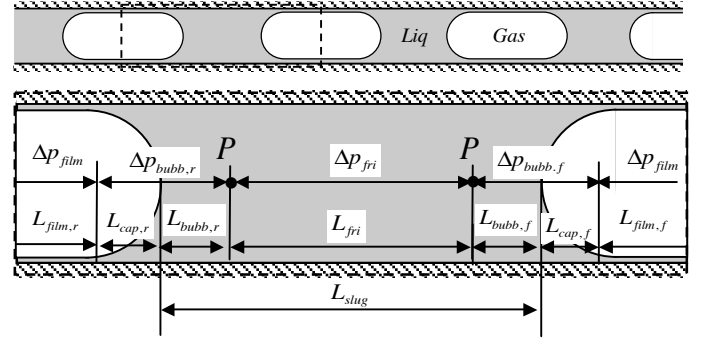


Fig. 4. Unit cell model

as numerical (Fukagata et al. 2007) studies. At the same time, the length and frequency of circulation inside the liquid slug determines the heat/mass transfer enhancement. Although empirical expressions have been proposed to correlate the bubble frequency and gas bubble length ratio with the gas/liquid superficial velocities (Garimela et al. 2002), their application is limited only to macro or millimeter tubes. For micro tubes, Hayashi et al. (2007) and Suo et al. (1964) have shown that a nozzle of different diameters used for gas inlet results in different bubble periods under the same superficial velocities. This feature raises extra obstacles in pressure drop modeling, while in the meantime it provides the possibility to achieve an optimized design of inlet geometries to improve heat transfer enhancement with a low cost of pressure drop.

To model the two-phase pressure drop with higher accuracy by accounting for the bubble frequency, a so-called unit cell model is proposed as illustrated in Fig. 4. The two-phase flow system from tube inlet to outlet is decomposed into several uniform unit cells. Each unit cell contains both a liquid slug and a gas bubble. The liquid slug is assumed to have no entrained gas as in macro-sized tubes. In view of the interface curvature, the gas bubble is composed of liquid film region, L_{film} , and two bubble caps, denoted as $L_{cap,r}$ and $L_{cap,f}$, respectively. Due to the strong surface tension, it is reasonable to assume that the liquid film is thin and uniform, while the caps are nearly hemispherical with $L_{cap,r} \approx L_{cap,f} \approx R$.

Accordingly, the total pressure drop of two-phase flow Δp_{TP} in a unit cell is the sum of the purely frictional pressure drop in the slug sandwiched by gas bubbles and the pressure drop over the gas bubble itself. The later can be further divided into the pressure drop in the liquid film and the pressure loss associated with front and rear caps of gas bubble, as illustrated in Fig. 2. The pressure components are correspondingly named as the friction pressure drop, Δp_{fri} , the film pressure drop, Δp_{film} , and the bubble pressure drop, Δp_{bubb} , respectively:

$$\Delta p_{TP} = \Delta p_{fri} + \Delta p_{film} + \Delta p_{bubb}, \quad \Delta p_{bubb} = \Delta p_{bubb,f} + \Delta p_{bubb,r}. \quad (22)$$

Concerning the film pressure drop Δp_{film} , under the premise of thin and uniform liquid film, the radiuses at the front and rear parts inside a gas bubble are the same. According to the Young-Laplace equation, the pressure jumps across interface is given as:

$$p_{bubb} - p_{film} = \frac{\sigma}{r_{int}}, \quad (23)$$

where the r_{int} is the radius of interface, p_{bubb} and p_{film} are the pressures at the gas bubble and liquid film, respectively. On the other hand, due to the negligible viscosity of gas phase, the pressure inside gas bubble is nearly uniform. It is straightforward that the pressure in liquid film is uniform, i.e., $\Delta p_{film} = 0$.

As indicated in Fig. 2, the frictional pressure drop Δp_{fri} can be simply predicted using the theoretical solution for Poiseuille flow, i.e., $fRe=64$. Accordingly,

$$\Delta p_{fri} = \frac{32\mu_L U_{TP}}{D^2} L_{fri}. \quad (24)$$

Note that the velocity employed here is U_{TP} because it is the real velocity at which the liquid moves in the tube. In addition, L_{fri} is the length over which the velocity profile can be described as a Poiseuille flow with a negligible error and differ from the visual liquid slug length L_{slug} .

Inside the liquid slug, there exist regions where velocity profile deviates from the parabolic profile, which are named as effecting bubble region hereafter. It contains two parts, $L_{bubb,f}$ and $L_{bubb,r}$ according to their relative positions to the gas bubble, and $L_{bubb} = L_{bubb,f} + L_{bubb,r}$. The visual liquid slug length, L_{slug} , can be expressed as $L_{slug} = L_{fri} + L_{bubb}$. The respective definitions and relationships are shown in Fig. 4.

The separating point between the effecting bubble region and the liquid single-phase region, denoted as ‘P’ in Fig. 4, is detected by using the relative magnitude of normal velocity. Numerical experiments have been carried out and it is found that when the relative normal velocity is less than 1% of the average two-phase flow, i.e.,

$$\left| \frac{u_r}{U_{TP}} \right| \leq 1\%, \quad (25)$$

the local fRe_{TP} deviates from 64 by only 1.5%.

Simulation has been further performed to evaluate the variation of the length of effective bubble region, L_{bubb} . The liquid slug is $4R$, which is long enough to get rid of the effects due to the interactions between two sequent gas bubbles. Figure 5 shows the variations of effecting bubble length against different Re_{TP} numbers. As shown in the figure, the effecting bubble length roughly equates one tube diameter and is nearly independent of Re_{TP} . Following a similar analysis method proposed by Fukagata et al. (2007), the magnitude of the effecting bubble length may be roughly estimated by considering that the normal and longitudinal velocities decay to zero with the same rate, i.e.,

$$\frac{u_r}{L_{bubb,f}} \sim \frac{u_r}{L_{bubb,r}} \sim \left| \frac{\partial u_z}{\partial r} \right|, \text{ and } \left| \frac{\partial u_z}{\partial r} \right| \sim \frac{U_{TP}}{R}. \quad (26)$$

Hence,

$$\frac{u_r}{U_{TP}} \sim \frac{L_{bubb}}{2R}. \quad (27)$$

Once the circulation in the liquid slug is formed, $u_r \sim U_{TP}$, therefore, $L_{bubb} \sim 2R$. This relation is confirmed analytically by Duda et al. (1970) and experimentally by Thulasidas et al. (1997).

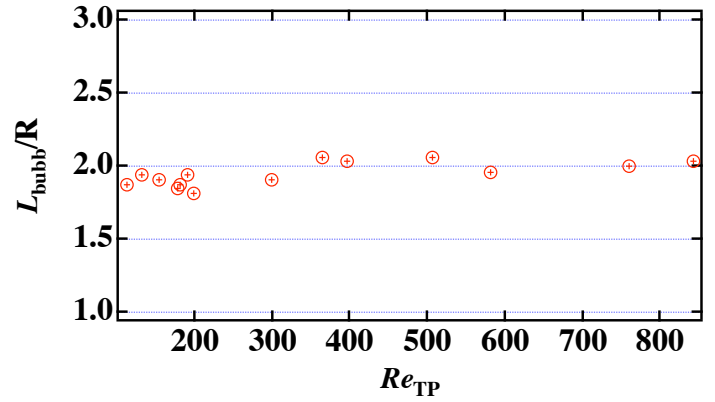


Fig. 5. Variations of bubble effective length against two-phase Re_{TP} number

Bubble Pressure Drop

Limited work is reported addressing the pressure drop over the front and rear capes of gas bubble. Bretherton (1961) pioneered the use of a lubrication analysis for the transition region between the spherical front of the bubble and the flat film far behind the cap. Expressions to predict the film thickness and pressure drop over the bubble were presented. In his model, the inertial force was neglected, while the variation of Ca number was implemented by changing the fluid viscosity. Kreutzer et al. (2005) experimentally studied the pressure drop over the bubble. Numerical simulations were also performed by using CFD package. The pressure drop over the gas bubble was converted to the liquid slug region with an extra term in the expression of fRe_{TP} as:

$$f = \frac{64}{Re_{TP}} \left[1 + b \frac{1}{L_{slug}} \left(\frac{Re_{TP}}{Ca} \right)^{0.33} \right]. \quad (28)$$

For $Re_{TP} < 50$ and $Re_{TP} \geq 50$, b takes different values of 0.07 and 0.17, respectively.

In the present study, once the velocity of two-phase reaches a steady state, the pressure drop over the gas bubble region are recorded and normalized by ρU_{TP}^2 . The variation of nondimensional pressure drop against the two-phase Re_{TP} number is shown in Fig. 6, while the results can be well

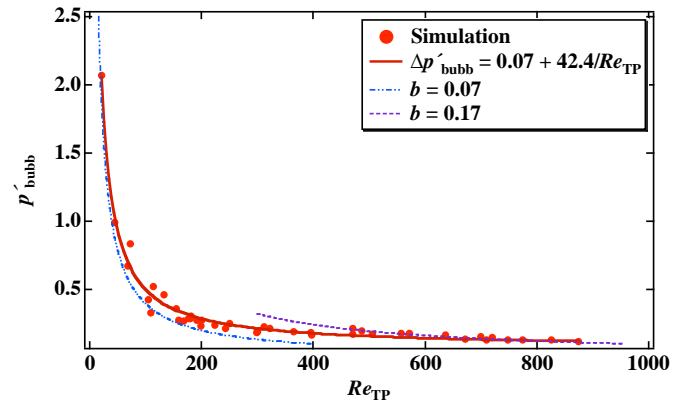


Fig. 6. Nondimensional pressures drop over the bubble against two-phase Re_{TP} number.

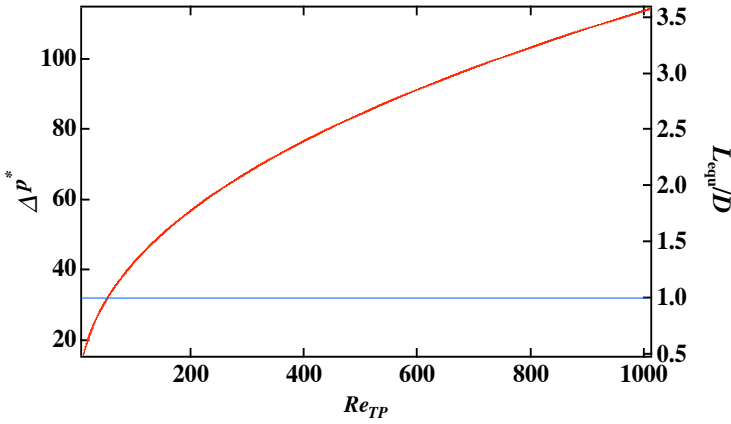


Fig. 7. Nondimensional bubble pressure drop and equivalent length.

correlated as:

$$\Delta p'_{bubb} = 0.07 + 42.4 / Re_{TP}. \quad (29)$$

For comparison, the results by Kreutzer et al. (2005) are also shown in the figure. Equation (29) shows the asymptotic changes toward the two limits of 0.07 and 0.17.

Pressure Drop Modeling

Based on Eq. (29), it is possible to roughly estimate the effect of gas bubble to the two-phase pressure drop. It is well known that the fully developed Poiseuille flow can be formulated as:

$$\frac{\partial p^*}{\partial z^*} = -32, \quad (30)$$

where the pressure and coordinate are normalized by $\mu u/D$ and D , respectively. Equation (30) means that the nondimensional pressure drop is 32 over a length of one tube diameter. Similarly, the bubble pressure drop $\Delta p'_{bubb}$ and the equivalent length in terms of tube diameter L_{eq}/D are shown in Fig. 7. The pressure drop increases dramatically with Re_{TP} and is roughly equivalent to the pressure drop over length of 0.5 ~ 3.5 times of the tube diameter in the developed single-phase flow. Taking $Re_{TP} = 500$ as an example, the dimensionless pressure drop is nearly 90, which is nearly the pressure drop over a length of three times tube diameters of a developed flow. When the gas bubble is short, the presence of a bubble will cause a measurable increase in the two-phase pressure drop. For a gas bubble of two times of the tube diameter, the global pressure drop can be simply formulated as a fully developed single-phase flow with velocity of U_{TP} .

Once each component of pressure drop is clarified, the two-phase pressure drop can be formulated and compared with the available models. The Lockhart-Martinelli model is a widely used method to evaluate the pressure drop of two-phase flow in macro-sized tubes. Originally, the relationship between Lockhart-Martinelli parameter X^2 and the friction multiplier, Φ_L^2 are graphically represented. They are defined respectively as:

$$\Phi_L^2 = \frac{(-dP/dz)_{TP}}{(-dP/dz)_{LO}}, \quad X^2 = \frac{(-dP/dz)_{LO}}{(-dP/dz)_{GO}}, \quad (31)$$

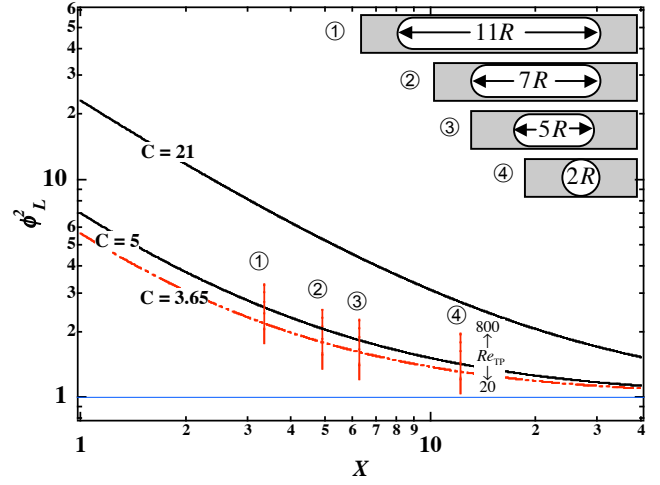


Fig. 8. Predicted pressure drop donated as Lockhart-Martinelli correlation for different gas bubble length.

where $(-dP/dz)_{LO}$ and $(-dP/dz)_{GO}$ are the pressure gradients required to drive single phase liquid and gas flows at the same superficial velocities, respectively. Later, Chisholm (1967) related the friction multiplier to the Lockhart-Martinelli parameter through a simple expression as follows:

$$\Phi_L^2 = 1 + \frac{C}{X} + \frac{1}{X^2}. \quad (32)$$

The L-M model has enjoyed success in predicting the two-phase drop in small channels. It was tested successfully for air-water flow in miniature triangular channels of $D_H = 0.87 - 2.89$ mm by Zhao & Bi (2001), and a circular tube of $D = 100 \mu\text{m}$ by Kawahara et al. (2002). Mishima & Hibiki (1996) suggested a modified expression of C by correlating their experimental data of air-water flow in tubes of 1 - 4 mm ID as:

$$C = 21[1 - \exp(-0.319D)], \quad (33)$$

where the diameter D is in millimeter. For the present case with $D = 0.6$ mm, Eq. (33) gives $C = 3.65$.

The unit cell model and bubble pressure drop correlation are integrated to predict the global two-phase pressure drop. The visual liquid slug length L_{slug} is fixed at $4R$, while the gas bubble is specified as $2R$, $5R$, $7R$ and $11R$, respectively. According to the definition shown in Fig. 4, and results in Fig. 5, the frictional liquid slug length L_{fri} is $2R$. The frictional pressure drop is calculated by using Eq. (24), while the U_{TP} is calculated from two-phase Re_{TP} number as:

$$U_{TP} = \frac{\mu_L Re_{TP}}{\rho_L D}. \quad (34)$$

The Re_{TP} number spans a wide range of 20 ~ 800. The bubble pressure Δp_{bubb} is calculated from Eq. (29), and the pressure over liquid film is negligible. Therefore, the global two-phase pressure drop is given as:

$$\Delta p_{TP} = \Delta p_{fri} + \Delta p_{bubb}. \quad (35)$$

To calculate X^2 and Φ_L^2 , the superficial liquid and gas velocities are required. Combining Eqs. (18) and (20), it comes:

$$j_G = \beta U_{TP} = 1.2\alpha U_{TP}, \quad j_L = U_{TP} - j_G. \quad (36)$$

where the void fraction, α , can be algebraically calculated from the volumes occupied respectively by liquid and gas phase.

The predicted results are shown in Fig. 8. The curves of Chisholm correlation with $C = 21$, $C = 5$ and $C = 3.65$ are also shown. The prediction covers the lines of $C = 5$ and 3.66 with the change in the Re_{TP} number. The discrepancy with the experimental correlation is due to the two limits of Re_{TP} number. Under those limit conditions, the related flow patterns are hardly achieved experimentally.

CONCLUSIONS

In the present work, a series of numerical simulation is carried out for air-water two-phase slug flows in a micro tube. The tube diameter is fixed at $600\ \mu\text{m}$. The Phase-Field method is employed to capture the interface, while the surface tension force is represented by the chemical potential formulation in order to suppress the significant parasitic flow. The two-phase Re_{TP} number is 20-800, while Ca number as 0.001-0.02, where the surface tension force is dominant.

A unit cell model is proposed to analyze the pressure drop, which consists components due to a gas bubble and a liquid slug. The local variation of the frictional factor shows that, apart from viscous and inertial forces, the bubble's two caps have a profound impact on the overall pressure drop. This indicates that the bubble frequency and relative bubble/slug length have significant effects on the two-phase pressure drop. Correspondingly, for the liquid flow of one tube diameter length away from gas bubble, the flow profile across the tube is almost identical to a Poiseuille flow and the corresponding pressure drop can be predicted by an analytical solution of $fRe_{TP} = 64$. The pressure drop along the liquid film is negligible under the condition that the liquid film is thin and uniform along the flow direction. The pressure drop due to gas bubble caps is determined by the two-phase Re_{TP} number, which is correlated as: $\Delta p'_{bubb} = 0.07 + 42.4 / Re_{TP}$.

The theoretical foundations with quantitative estimate indicate the importance of the bubble frequency. However, the gas bubble length is not solely determined by the two-phase superficial velocities, the inlet geometry also has a profound impact. This may partly explain the reason why the available experimental results are correlated in the form of homogenous or separated two-phase models without accounting for the bubble frequency. The inlet effect for two-phase flow in a micro tube also provides the possibility and direction for optimization.

The proposed model and correlation are assembled to predict slug flows with four different gas bubble lengths. The Re_{TP} number spans a sufficient wide range. The predicted two-phase multiplier covers the curves of laminar flow in macro tube and the one proposed for millimeter tubes. Further studies should be needed to clarify the effect of different bubble shape and slip velocity between the gas and liquid phase.

ACKNOWLEDGMENTS

The authors are grateful to Drs. Y. Hasegawa, Y. Suzuki and N. Shikazono (The University of Tokyo), for fruitful discussions and comments. This work was supported through the 21st Century COE Program, Mechanical Systems

Innovation, by the Ministry of Education, Culture, Sports, Science and Technology of Japan (MEXT).

REFERENCES

- Amador, C., Salman, W., Sanguanpiyapan, S. et al., 2004. Effect of Gas/Liquid Inlet Conditions on the Mechanism of Taylor Flow Formation. *5th Int. Conf. Multiphase Flow*, Yokohama, May. 30 – Jun. 4.
- Anderson, D. M., McFadden, G. B. and Wheeler, A. A., 1998. Diffuse-interface methods in fluid Mechanics. *Annu. Rev. Fluid Mech.* 30, 139-165.
- Baten, J. M. and Krishna, R., 2005. CFD simulations of Wall Mass Transfer for Taylor Flow in Circular Capillaries. *Chem. Eng. Sci.* 60, 1117-1126.
- Bretherton, F. P., 1961. The motion of long bubbles in tube. *J. Fluid. Mech.* 10, 166-188.
- Chisholm, D., 1967. A theoretical basis for the Lockhart-Martinelli correlation for two-phase flow. *Int. J. Heat Mass Transfer* 10, 1767-1778.
- Duda, J. L. and Vrentas, J. S., 1970. Steady flow in the region of closed streamlines in a cylindrical cavity. *J. Fluid. Mech.* 45, 247-260.
- Fukano T., and Kariyasaki A., 1993. Characteristics of gas-liquid two-phase flow in a capillary tube. *Nucl. Eng. Des.* 141, 59-68.
- Fukagata, K., Kasagi, N., Ua-arayaporn P. and Himeno, T., 2007. Numerical Simulation of Gas-Liquid Two-Phase Flow and Convective Heat Transfer in a Micro Tube. *Int. J. Heat and Fluid Flow* 28, 72-82.
- Garimella, S., Killion, J.D. and Coleman, J.W., 2002. An experimentally validated model for two-phase pressure drop in the intermittent flow regime for circular microchannels. *J. Fluids Eng. –Trans. ASME* 124, 205-214.
- Ghiaasia, S. M. and Abdel-khalik, S. I., 2001. Two-Phase Flow in Microchannels. *Advances in Heat Transfer* 34, 145-254.
- Hayashi, S., Kasagi, N. and Suzuki, Y., 2007. The effects of inlet flow conditions on gas-liquid two-phase flow in a micro tube. *ASME-JSME Therm. Eng. Summer Heat Transfer Conf.*, Vancouver, July 8-12, No. HT2007-32916
- He, Q.W. and Kasagi, N., 2008. Phase-Field Simulation of Small Capillary-Number Two-Phase Flow in a Micro Tube. *Fluid Dyn. Res.* accepted.
- Irlandous, S. and Andersson, B., 1989. Liquid film in Taylor flow through a capillary. *Ind. Eng. Chem. Res.* 28, 1684-1692.
- Jacqmin, D., 1999. Calculation of Two-Phase Navier-Stokes Flows Using Phase-Field Modeling. *J. Comput. Phys.* 155, 96-127.
- Kawahara, A., Chung, P.M.-Y. and Kawaji, M., 2002. Investigation of two-phase flow pattern, void fraction and pressure drop in a microchannel. *Int. J. Multiphase Flow* 28, 1411-1435.
- Kreutzer, M.T., Kapteijn F. et al., 2005. Inertial and Interfacial Effects on Pressure Drop of Taylor Flow in Capillaries. *AIChE J.* 51, 2428-2440.
- Mishima, K. and Hibiki, T., 1996. Some characteristics of air-water two-phase flow in small diameter vertical tubes. *Int. J. Multiphase Flow* 22, 703-723.

- Saisorn S. and Wongwises S., 2007. Flow pattern, void fraction and pressure drop of two-phase air-water flow in a horizontal circular micro-channel. *Exp. Therm. Fluid Sci.* 32, 748-760.
- Shirani, E., Ashgriz, N. and Mostaghimi, J., 2005. Interface pressure calculation based on conservation of momentum for front capturing methods. *J. Comput. Phys.* 203, 154-175.
- Son, G., Dhir, V. K., and Ramanujapu, N. K., 1999. Dynamics and Heat Transfer Associated with a Single-Bubble Nucleate Boiling on a Horizontal Surface. *J. Heat Transfer* 121, 623-631.
- Suo, M. and Griffith, P., 1964. Two-phase flow in capillary tubes. *J. Basic Eng.* 86, 576-582.
- Taylor, G.I., 1961. Deposition of a viscous fluid on the wall of a tube. *J. Fluid Mech.* 10, 161-165.
- Thulasidas, T.C., Abraham, M. A. and Cerro, R. L., 1997. Flow pattern in liquid slugs during bubble-train flow inside capillaries. *Chem. Eng. Sci.* 52, 2947-2962.
- Yabe, T., Aoki, T., Sakiguchi, G. et al., 1991. The compact CIP (Cubic-Interpolated Pseudo-particle) method as a general hyperbolic solver. *Comput. Fluids* 19, 421-431.
- Zhao, T.S. and Bi, Q.C., 2001. Co-current air-water two-phase flow patterns in vertical triangular microchannels. *Int. J. Multiphase Flow* 27, 765-782.